Midinfrared optical frequency comb based on difference frequency generation using high repetition rate Er-doped fiber laser with single wall carbon nanotube film

M. Tsuzuki,[1] L. Jin,[1] M. Yamanaka,[1] V. Sonnenchein,[1] H. Tomita,[1] A. Sato,[2] T. Ohara,[2] Y. Sakakibara,[3] E. Omoda,[3] H. Kataura,[3] T. Iguchi,[1] and N. Nishizawa[1,*]

[1]*Department of Quantum Engineering, Nagoya University, Nagoya 464-8603, Japan*
[2]*Sekisui Medical Co. Ltd., Ibaraki 319-1182, Japan*
[3]*National Institute of Advanced Industrial Science and Technology (AIST), Tsukuba 305-8565, Japan*
**Corresponding author: nishizawa@nuee.nagoya-u.ac.jp*

Received August 11, 2016; revised October 12, 2016; accepted October 27, 2016;
posted October 27, 2016 (Doc. ID 273614); published November 28, 2016

We demonstrated stable midinfrared (MIR) optical frequency comb at the 3.0 μm region with difference frequency generation pumped by a high power, Er-doped, ultrashort pulse fiber laser system. A soliton mode-locked 161 MHz high repetition rate fiber laser using a single wall carbon nanotube was fabricated. The output pulse was amplified in an Er-doped single mode fiber amplifier, and a 1.1–2.2 μm wideband supercontinuum (SC) with an average power of 205 mW was generated in highly nonlinear fiber. The spectrogram of the generated SC was examined both experimentally and numerically. The generated SC was focused into a nonlinear crystal, and stable generation of MIR comb around the 3 μm wavelength region was realized.

OCIS codes: (140.3070) Infrared and far-infrared lasers; (060.2320) Fiber optics amplifiers and oscillators.
http://dx.doi.org/10.1364/PRJ.4.000313

1. INTRODUCTION

In the midinfrared (MIR) region, there are a variety of absorption spectra of fundamental vibration bands of molecular gases. Such absorption spectra have precise structures, and this region is called the finger print region. Thus MIR spectroscopy allows us to identify and quantify molecular species in a sample.

For the MIR spectroscopy, the Fourier transform infrared spectroscopy with lamp light sources has been generally used. The optical frequency comb based techniques enable high speed molecular sensing with ultrahigh accuracy [1]. Several applications have been investigated in the fields of fundamental research, industries, biomedicine, environmental sensing, and so forth [1,2]. Nowadays, the development of a robust and practical MIR comb is desired to realize highly sensitive and highly accurate molecular identification.

Fiber laser based combs are attractive for their stable, practical, and reliable performances. So far, MIR comb generation pumped by fiber lasers has been demonstrated by several groups. The difference frequency generation (DFG) pumped by Er- [3–5] and Yb-doped fiber laser systems [6,7], and optical parametric oscillator (OPO) [8–11] have been used to achieve MIR comb generation around the 3 μm wavelength region.

Single wall carbon nanotube (SWNT) is one of the attractive devices as the saturable absorber of ultrashort pulse fiber lasers [12–15]. It has fast temporal response of ~1 ps and wide operation bandwidth. It is also easy to fabricate a transmission type device, which is useful for ultrashort pulse fiber lasers. Using the combination of highly nonlinear fiber, we can generate wideband supercontinuum (SC), which works as a broadband coherent laser source [16,17].

In this work, we demonstrated MIR comb generation using an Er-doped SWNT fiber laser based system. A high power, ultrashort pulse with high repetition frequency of 161 MHz was generated by an SWNT fiber laser and fiber amplifier. A widely broadened SC was generated with highly nonlinear fiber and high power, ultrashort pulse. The characteristics of the generated SC were examined both experimentally and numerically, and the fiber length was optimized in terms of MIR comb generation. The generated SC was focused onto the nonlinear crystal, and the offset-free MIR comb was generated around the 3 μm wavelength range through DFG. The developed system was an almost all-fiber configuration, and the stable generation of MIR comb was realized.

2. EXPERIMENTAL SETUP AND HIGH POWER, ULTRASHORT PULSE GENERATION

Using the OPO, although we can achieve a high power MIR comb, it needs synchronized feedback control [8–11]. Using the DFG, the offset frequency f_{ceo} is canceled out by the subtraction, and an offset-free MIR comb can be achieved [18,19]. However, the conversion efficiency is not high, and we have to prepare high power seed pulses. In this work, we used the DFG process to generate the MIR comb.

Figure 1 shows the experimental setup of MIR comb generation. We started from a high repetition rate, ultrashort pulse fiber laser. The high power, ultrashort pulse was generated with a fiber amplifier and dispersion compensation fiber. Then a wideband SC was generated, and the MIR comb was achieved from DFG of SC. The system consists of almost

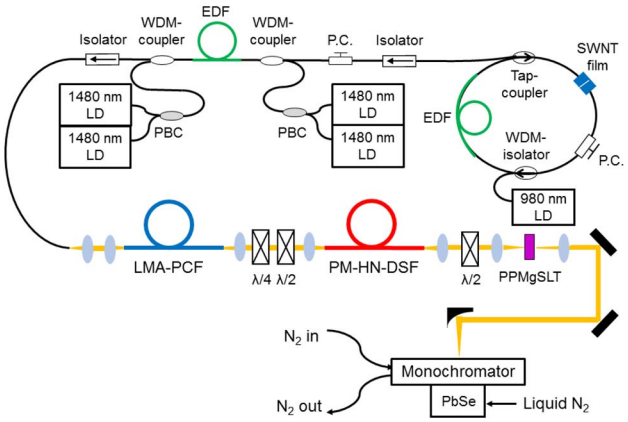

Fig. 1. Experimental setup of MIR comb generation based on Er-doped, ultrashort pulse fiber laser system.

all-fiber systems, and a frequency stabilized MIR comb can be achieved stably.

As the seed pulse source, we made passively mode-locked, Er-doped, ultrashort pulse fiber laser with an SWNT saturable absorber [13,14]. The SWNT was synthesized by the laser ablation method, and the diameter of 1.2 nm was obtained selectively. The SWNT was equally dispersed in polyimide liquid, and a free-standing polyimide film was fabricated by water evaporation. The SWNT polyimide film was easily inserted between the fiber connectors inside the fiber laser cavity, and it works as a fast and wideband mode locker.

The fiber laser cavity consists of nonpolarization maintaining single mode fiber devices. In order to achieve the wide comb mode spacing, we made a high repetition rate, ultrashort pulse fiber laser. A 0.5 m length of Er-doped fiber (EDF) pumped by a high power laser diode (LD) at 980 nm wavelength was used as the gain medium. The polarization controller, optical isolator, and output coupler were used to construct the cavity. The net cavity dispersion was -0.28×10^{-3} ps^2.

Figure 2 shows the characteristics of the output pulse from the fiber laser. The temporal shape and chirping property

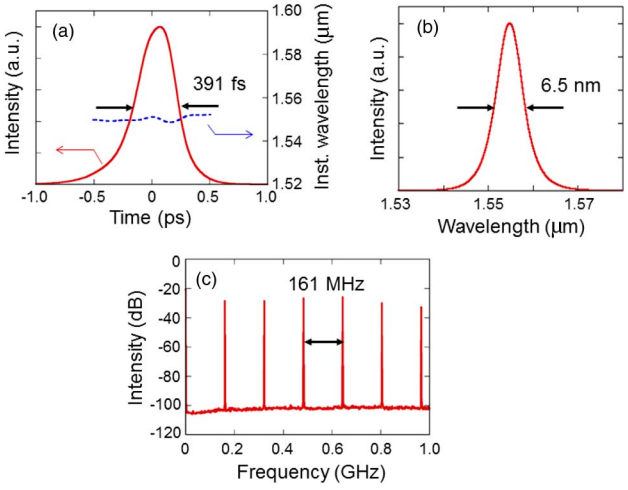

Fig. 2. Characteristics of output pulse from fiber laser: (a) temporal shape with instantaneous wavelength, (b) optical spectrum, and (c) RF spectra.

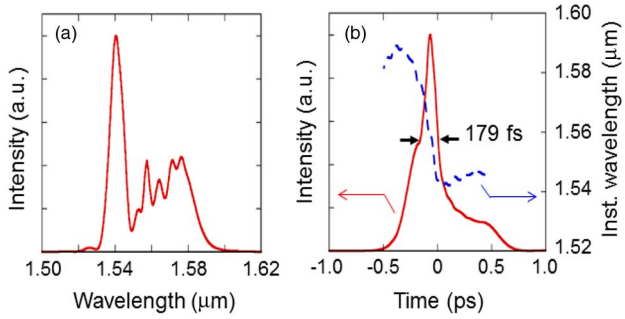

Fig. 3. Characteristics of output pulse from fiber amplifier: (a) optical spectrum and (b) temporal shape with instantaneous wavelength.

were observed with a frequency resolved optical gating (FROG) [20]. An almost transform limited, clean, ultrashort pulse with temporal width of 391 fs was achieved. The pulse spectrum had also a clean sech^2-like shape with a spectral width of 6.5 nm. For the RF spectra, a clean RF spectral train with 161 MHz equal spacing was observed clearly and stably, and the stable passive mode locking was confirmed. The average power was 11 mW.

The output pulse from the fiber laser was introduced into an EDF amplifier, which consists of high concentration EDF with positive dispersion property. Four high power LDs at 1480 nm wavelength were used as the pump laser. The average power was increased from 11 to 420 mW. Figure 3 shows the optical spectrum and temporal shape of the output pulse from the fiber amplifier. A 172 fs high power short pulse with large upchirping was observed at the output of the EDF amplifier.

Then we applied dispersion compensation using a large mode field area photonic crystal fiber (LMA-PCF, LMA30). Using the LMA-PCF, we demonstrated dispersion compensation effectively while suppressing the nonlinear effect. The magnitude of second order dispersion β_2 was -32 ps^2/km, and the mode-field diameter was 25 μm. The length of the LMA-PCF was optimized by the cut-back method and FROG measurement.

Figure 4 shows the temporal shape of the dispersion compensated ultrashort pulse when 50 cm of LMA-PCF was used. An almost chirp-free ultrashort pulse was generated. The temporal width was 102 fs at FWHM, and the estimated peak power of the output pulse was 17 kW.

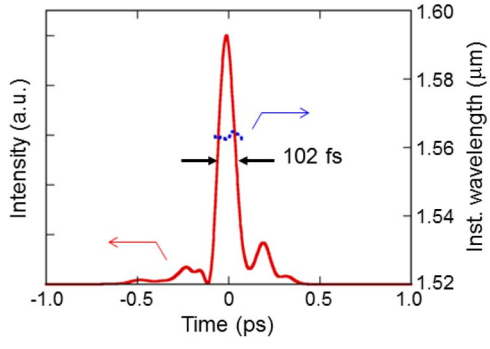

Fig. 4. Temporal shape and instantaneous wavelength of dispersion compensated ultrashort pulse with LMA-PCF.

3. GENERATION OF SC AND MIR COMB

Next, in order to generate the optical frequency comb at the MIR region by DFG, we generated SC. A polarization maintaining, highly nonlinear, dispersion shifted fiber (PM-HN-DSF) was used as the nonlinear device [21]. The zero-dispersion wavelength was 1.55 μm, and the mode-field diameter was 3.0 μm. The magnitude of the dispersion parameter $D = 1.0$ ps/km/nm, and dispersion slope $D' = 0.03$ ps/km/nm^2 at a wavelength of 1.55 μm.

In order to examine the optimum fiber length, we demonstrated the numerical analysis of SC generation. Figure 5 shows the numerical results of SC generation using a high power, ultrashort pulse and PM-HN-DSF when the fiber length was 10, 20, and 30 cm. The extended nonlinear Schrödinger equation was used for the analysis [22]. A 100 fs, sech^2-shaped, transform limited, ultrashort pulse with a peak power of 17 kW was assumed as the input pulse. At the short length of propagation, the spectrum broadening was mainly induced by self-phase modulation [21]. As shown in Fig. 5, the spectral width was broadened as the fiber length was increased. The temporal width was also increased for the fiber length increment. From Fig. 5, we can see that a broadband spectrum with enough bandwidth and small temporal broadening was generated when the fiber length was 20 cm. Considering the smooth spectral shape of SC and the short length of PM-HN-DSF, the high coherence property is expected [23,24]. As a result, we decided that the optimum length of PM-HN-DSF was 20 cm in order to generate the seed SC pulse of MIR comb generation through DFG.

Figure 6 shows the observed optical spectrum of generated SC in 20 cm of PM-HN-DSF. The wideband SC, broadened from 1.1 to 2.1 μm, was generated stably. The observed spectrum was similar to the numerical one. The average power was 205 mW.

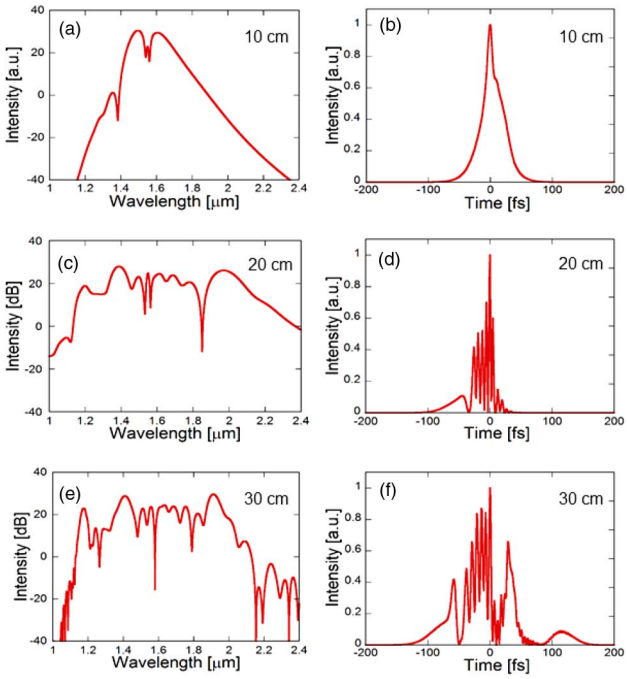

Fig. 5. (a), (c), and (e) optical spectra and (b), (d), and (f) temporal shape of output pulse from highly nonlinear fiber for the length of 10, 20, and 30 cm.

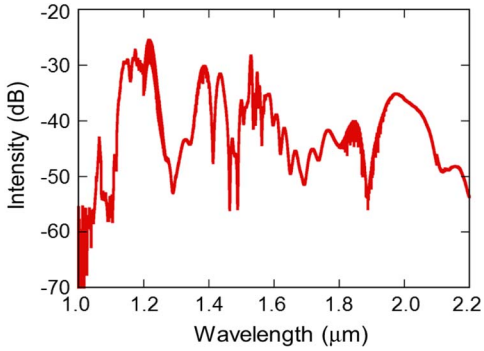

Fig. 6. Observed optical spectrum of generated SC in PM-HN-DSF.

Figure 7 shows the spectra of the SWNT measured noise fiber laser and the generated SC. The intensity noise was characterized using a fast photodiode, a bias tee, and an RF spectrum analyzer. Although there was a peak around 2 MHz, the noise level was low, and there was no large noise component. The magnitude of noise was not increased during the SC generation process.

Next, we examined the coherence properties of the generated SC by the balanced heterodyne RF beat measurement. Figure 8 shows the observed RF beat between the stable cw-LD and fiber laser SC. The output beams from the cw-LD and the examined laser beam were overlapped in a single mode fiber coupler. Then the overlapped beams were introduced into a balanced photodetector, and the output signal was observed with an RF spectrum analyzer. Narrow bandpass filters with the bandwidth of 0.6–1.0 nm were used to pick off the spectral component for RF beat detection. We used two stable cw-LDs as the reference beam (LIO [$\lambda = 1550$ nm], and Santec [$\lambda = 1680$ nm]). Figure 8 shows the observed RF beat note between cw-LDs and the fiber laser and SC. The f_{beat} components were observed with a high signal to noise ratio larger than 30 dB for all three measurements. We confirmed the high coherence of the fiber laser and generated SC.

Next, in order to investigate the feasibility of MIR comb generation using the generated SC, we observed temporal distribution of spectral components using the cross-correlation FROG (X-FROG) [20,25,26]. The generated SC was introduced into a sum frequency generation type autocorrelation FROG system. A long pass filter was used in one arm of the FROG,

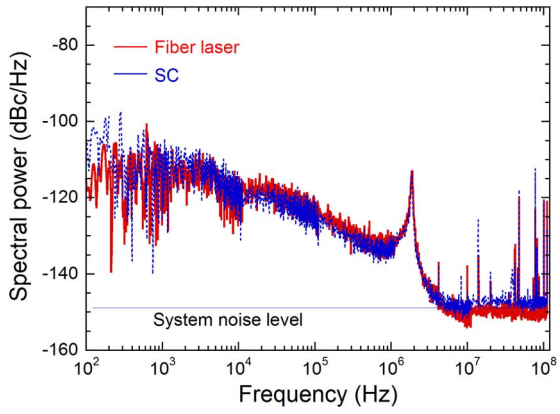

Fig. 7. Observed RF noise of fiber laser output and SC.

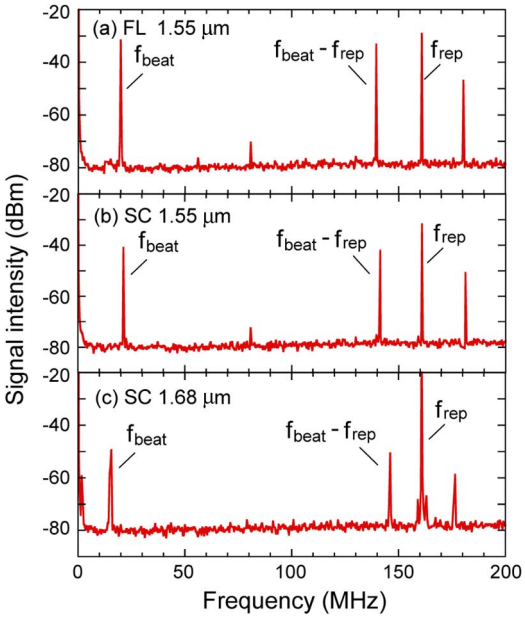

Fig. 8. Observed RF beat notes between cw-LD and (a) fiber laser at 1550 nm, (b) SC at 1550 nm, and (c) SC at 1680 nm.

and the longer wavelength side was picked off and used as the probe pulse. A 1 mm thick BaB_2O_4 crystal was used as the $\chi^{(2)}$ medium.

Figure 9(a) shows the observed X-FROG trace of the generated SC in 20 cm of PM-HN-DSF. Although the spectrogram was tilted a little by the effect of chirping of the probe pulse, we observed the temporal distribution of spectral components.

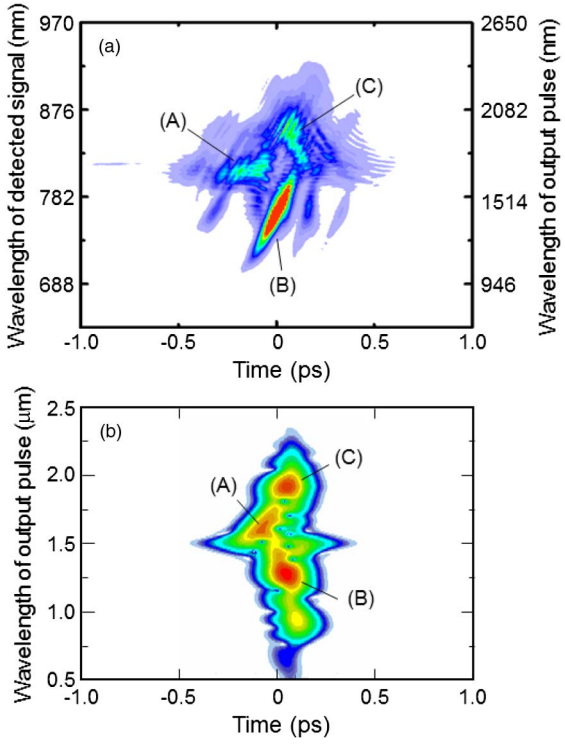

Fig. 9. Spectrogram of generated SC in 20 cm of highly nonlinear fiber; (a) experimentally observed spectrogram with X-FROG, and (b) numerically obtained spectrogram with PG-FROG.

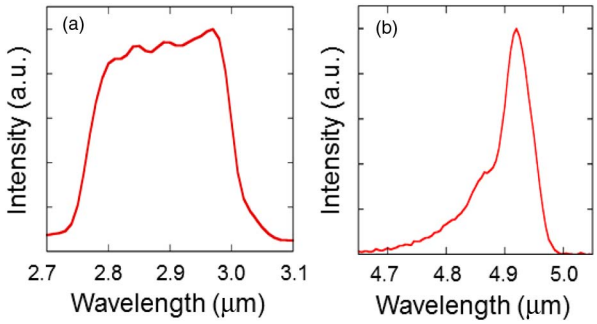

Fig. 10. Observed optical spectra of generated MIR comb at wavelengths of (a) 2.9 and (b) 4.9 μm.

It was considered that the interference components were caused by the multiple reflections at the wavelength filter and optical devices in the X-FROG system. Figure 9(b) shows the numerical result. The polarization gating type X-FROG (PG-FROG) was used to achieve the spectrogram in the numerical analysis [20]. Here a 100 fs, sech^2-shaped pulse was assumed as the probe pulse. The numerical result shows a similar distribution to the experimental one, and the three peaks shown with symbols (A)–(C) were observed both in the experimental result and the numerical one. From Fig. 9, we can see that the main components were almost overlapped temporally. This means that we can achieve the MIR comb generation by only focusing the generated SC into the DFG crystal.

Next, we focused the generated SC into a nonlinear crystal. In this work, we used fan-out type periodically poled MgSLT (PPMgSLT). The PPMgSLT was designed to generate an MIR comb at the 3.0–5.0 μm region by a 1.3–1.8 μm near-infrared pulse. The length and thickness of the crystal were 11 and 1.0 mm, respectively.

Figure 10 shows the observed optical spectra of the generated MIR comb. The spectra were observed with a monochromator and PbSe detector. The MIR combs were observed stably at 2.9 and 4.9 μm wavelength regions. The observed average power of the 2.9 μm component was 512 μW, and that of 4.9 μm was ~100 μW. The wavelength of 2.9 μm matched to the DFG wavelength between components (B) and (C), and that of 4.9 μm matched to the DFG between components (A) and (B) in Fig. 9. The MIR comb was observed stably for more than 48 h without any maintenance.

Thanks to the high coherence property of the SC generated in a short PM-HN-DSF, the high temporal coherence of obtained MIR comb is expected. Recently, we directly confirmed the high coherence property of the MIR comb pumped with a coherent SC generated in a Yb-doped fiber laser system [27].

4. CONCLUSION

In conclusion, we demonstrated MIR optical frequency comb generation at the 3.0 μm region by DFG pumped by a high power fiber laser SC. A soliton mode-locked, 161 MHz, high repetition rate EDF laser was constructed using SWNT film. Then a 102 fs, 17 kW, high power, ultrashort pulse was generated using fiber amplifier and large mode field area fiber. Considering the numerical result, a 1.1–2.2 μm wideband SC was generated for the DFG. The spectrogram of generated SC was examined both experimentally and numerically, and the temporal distribution of spectral components was

confirmed. Then the generated SC was focused into the nonlinear crystal, and the stable generation of an MIR comb around 2.9 and 4.9 μm wavelength regions was realized. The developed system consists of almost all-fiber devices, and it is useful for practical applications. Further power scaling is under investigation.

Funding. Japan Science and Technology Agency (JST); Japan Agency for Medical Research and Development (AMED).

Acknowledgment. This research is partially supported by the SENTAN program "Development of Systems and Technology for Advanced Measurement and Analysis" of the JST, and the AMED.

REFERENCES

1. A. Schliesser, N. Picque, and T. W. Hansch, "Mid-infrared frequency combs," Nat. Photonics **6**, 440–449 (2012).
2. M. J. Thorpe, D. Balslev-Clausen, M. S. Kirchner, and J. Ye, "Cavity-enhanced optical frequency comb spectroscopy: application to human breath analysis," Opt. Express **16**, 2387–2397 (2008).
3. C. Erny, K. Moutzouris, J. Biegert, D. Kühlke, F. Adler, A. Leitenstorfer, and U. Keller, "Mid-infrared difference-frequency generation of ultrashort pulses tunable between 3.2 and 4.8 um from a compact fiber source," Opt. Lett. **32**, 1138–1140 (2007).
4. A. Gambetta, R. Ramponi, and M. Marangoni, "Mid-infrared optical combs from a compact amplified Er-doped fiber oscillator," Opt. Lett. **33**, 2671–2673 (2008).
5. F. Zhu, H. Hundertmark, A. A. Kolomenskii, J. Strohaber, R. Holzwarth, and H. A. Schuessler, "High-power mid-infrared frequency comb source based on a femtosecond Er:fiber oscillator," Opt. Lett. **38**, 2360–2362 (2013).
6. T. W. Neely, T. A. Johnson, and S. A. Diddams, "High-power broadband laser source tunable from 3.0 to 4.4 μm based on a femtosecond Yb:fiber oscillator," Opt. Lett. **36**, 4020–4022 (2011).
7. S. A. Ruehl, A. Gambetta, I. Hartl, M. E. Fermann, K. S. E. Eikema, and M. Marangoni, "Widely-tunable mid-infrared frequency comb source based on difference frequency generation," Opt. Lett. **37**, 2232–2234 (2012).
8. F. Adler, K. C. Cossel, M. J. Thorpe, I. Hartl, M. E. Fermann, and J. Ye, "Phase-stabilized, 1.5 W frequency comb at 2.8–4.8 μm," Opt. Lett. **34**, 1330–1332 (2009).
9. N. Leindecker, A. Marandi, R. L. Byer, and K. L. Vodopyanov, "Octave-spanning ultrafast OPO with 2.6–6.1 μm instantaneous bandwidth pumped by femtosecond Tm-fiber laser," Opt. Express **20**, 7046–7053 (2012).
10. K. F. Lee, J. Jiang, C. Mohr, J. Bethge, M. E. Fermann, N. Leindecker, K. L. Vodopyanov, P. G. Schunemann, and I. Hartl, "Carrier envelope offset frequency of a doubly resonant, nondegenerate, mid-infrared GaAs optical parametric oscillator," Opt. Lett. **38**, 1191–1193 (2013).
11. N. Coluccelli, H. Fonnum, M. Haakestad, A. Gambetta, D. Gatti, M. Marangoni, P. Laporta, and G. Galzerano, "250-MHz synchronously pumped optical parametric oscillator at 2.25–2.6 μm and 4.1–4.9 μm," Opt. Express **20**, 22042–22047 (2012).
12. Y.-C. Chen, N. R. Raravikar, L. S. Schadler, P. M. Ajayan, Y.-P. Zhao, T.-M. Lu, G.-C. Wang, and X.-C. Zhang, "Ultrafast optical switching properties of single-wall carbon nanotube polymer composites at 1.55 μm," Appl. Phys. Lett. **81**, 975–977 (2002).
13. N. Nishizawa, Y. Seno, K. Sumimura, Y. Sakakibara, E. Itoga, H. Kataura, and K. Itoh, "All-polarization-maintaining Er-doped ultrashort pulse fiber laser using carbon nanotube saturable absorber," Opt. Express **16**, 9429–9435 (2008).
14. Y. Senoo, N. Nishizawa, Y. Sakakibara, K. Sumimura, E. Itoga, H. Kataura, and K. Itoh, "Polarization-maintaining, high-energy, wavelength-tunable, Er-doped ultrashort pulse fiber laser using carbon-nanotube polyimide film," Opt. Express **17**, 20233–20241 (2009).
15. S. Yamashita, "A tutorial on nonlinear photonic applications of carbon nanotube and graphene," J. Lightwave Technol. **30**, 427–447 (2012).
16. N. Nishizawa, "Generation and application of high-quality supercontinuum sources," Opt. Fiber Technol. **18**, 394–402 (2012).
17. N. Nishizawa, "Ultrashort pulse fiber lasers and their applications," Jpn. J. Appl. Phys. **53**, 090101 (2014).
18. H. R. Telle, G. Steinmeyer, A. E. Dunlop, J. Stenger, D. H. Sutter, and U. Keller, "Carrier-envelope offset phase control: a novel concept for absolute optical frequency measurement and ultrashort pulse generation," Appl. Phys. B **69**, 327–332 (1999).
19. Y. Deng, F. Lu, and W. H. Knox, "Fiber-laser-based difference frequency generation scheme for carrier-envelope-offset phase stabilization applications," Opt. Express **13**, 4589–4593 (2005).
20. R. Trebino, *Frequency Resolved Optical Gating: The Measurement of Ultrashort Laser Pulses* (Kluwer, 2000).
21. N. Nishizawa and T. Goto, "Widely broadened super continuum generation using highly nonlinear dispersion shifted fibers and femtosecond fiber laser," J. Appl. Phys. **40**, L365–L367 (2001).
22. G. P. Agrawal, *Nonlinear Fiber Optics*, 4th ed. (Academic, 2007).
23. J. M. Dudley, G. Genty, and S. Coen, "Supercontinuum generation in photonic crystal fiber," Rev. Mod. Phys. **78**, 1135–1184 (2006).
24. T. Hori, N. Nishizawa, T. Goto, and M. Yoshida, "Experimental and numerical analysis of widely broadened supercontinuum generation in highly nonlinear dispersion-shifted fiber with a femtosecond pulse," J. Opt. Soc. Am. B **21**, 1969–1980 (2004).
25. N. Nishizawa and T. Goto, "Experimental analysis of ultrashort pulse propagation in optical fibers around zero-dispersion region using cross-correlation frequency resolved optical gating," Opt. Express **8**, 328–334 (2001).
26. A. Okamura, Y. Sakakibara, E. Omoda, H. Kataura, and N. Nishizawa, "Experimental analysis of coherent supercontinuum generation and ultrashort pulse generation using cross-correlation frequency resolved optical gating (X-FROG)," J. Opt. Soc. Am. B **32**, 400–406 (2015).
27. L. Jin, M. Yamanaka, V. Sonnenschein, H. Tomita, T. Iguchi, A. Sato, A. Omori, A. Ideno, T. Oh-hara, and N. Nishizawa, "Highly coherent tunable mid-infrared optical frequency comb pumped by supercontinuum at 1 μm," in *Laser Congress (ASSL)*, OSA Technical Digest (Optical Society of America, 2016), paper ATh1A.7.